Firoozy, N., Neusitzer, T., Desmond, D. S., Tiede, T., Lemes, M. J. L., Landy, J., ... Barber, D. G. (2017). An electromagnetic detection case study on crude oil injection in a young sea ice environment. *IEEE Transactions on Geoscience and Remote Sensing*, *55*(8), 4465-4475. https://doi.org/10.1109/TGRS.2017.2692734

An Electromagnetic Detection Case Study on Crude Oil Injection in a Young Sea Ice Environment

Nariman Firoozy, *Member, IEEE,* Thomas Neusitzer, *Student Member, IEEE,* Durell Desmond, Tyler Tiede, Marcos Lemes, Jack Landy, *Member, IEEE,* Puyan Mojabi, *Member, IEEE,* Søren Rysgaard, Gary Stern, and David G. Barber

***Abstract*—This paper presents a multidisciplinary case study on a crude oil injection experiment in an artificially-grown young sea ice environment under controlled conditions. In particular, the changes in the geophysical and electromagnetic responses of the sea ice to oil introduction are investigated for this experiment. Furthermore, we perform a preliminary study on the detection of oil spills utilizing the normalized radar cross section (NRCS) data collected by a C-band scatterometer is presented. To this end, an inversion scheme is introduced that retrieves the effective complex permittivity of the domain prior and post oil injection by comparing the simulated and calibrated measured NRCS data while roughness parameters calculated using lidar are utilized as prior information. Once the complex permittivity values are obtained, the volume fraction of oil within the sea ice is found using a mixture formula. Based on this volume fraction, a binary detection of oil presence seems to be possible for this test case. Finally, the possible sources of error in the retrieved effective volume fraction, which is an over-estimate of the actual value, are identified and discussed by a macro- and micro-level analyses through bulk salinity measurements and x-ray imagery of the samples, as well as a brief chemical analysis.**

***Index Terms*—crude oil, arctic, remote sensing, electromagnetic scattering**

I. Introduction

CLIMATE change has reduced the minimum Arctic sea ice extent by approximately 9.4 to 13.6% per decade from 1979 to 2012 [1]. This has led to the opening of new sea routes, and a renewed interest in the Northwest Passage in Canada [2]. Although this change in the Arctic transportation offers new economic opportunities, it comes with the risk of crude oil spills, and other transportation-related contaminants (*e.g.*, bunker fuel). Such spills need to be properly dealt with. The first step in responding to such a spill is the ability to detect its occurrence. The detection of a spill further allows us to enforce the environmental protection regulations by identifying the violators, and holding them accountable. But despite notable research on the impact and detection of oil spills [3], [4], this detection science and its associated technology need to be further improved [5].

Manuscript received xxxx. xx, 2017; revised xxxx. xx, 2017.

N. Firoozy, D. Desmond, M. Lemes, G. Stern, Søren Rysgaard, and D. G. Barber are with the Centre for Earth Observation Science, University of Manitoba, Winnipeg, MB, R3T 5V6, Canada (e-mail: firoozyn@myumanitoba.ca).

T. Neusitzer, T. Tiede, and P. Mojabi are with the Department of Electrical and Computer Engineering, University of Manitoba, Winnipeg, MB, R3T 5V6, Canada.

J. Landy is with the Bristol Glaciology Centre, School of Geographical Sciences, University of Bristol, Bristol, BS8 1SS, U.K.

The topic of oil slick detection in open waters has received significant attention [6]. In the microwave frequency range, SAR data with single polarization has been utilized to detect oil spills via the use of backscattering strength accompanied with setting signal thresholds based on prior information [7]. Regarding polarimetric SAR, an excellent review of various quad-, dual-, and compact-polarimetric methods is presented in [8]. Most polarimetric parameters are used to detect the deviation of oil slick scattering from the Bragg scattering behavior of the open water [9]. Regarding quad-polarimetric methods, the parameters of entropy, anisotropy, mean scattering angle, covariance scaling factor, degree of polarization, and normalized pedestal height have successfully been utilized for oil slick detection in open water before [9]–[12]. In the case of dual-polarimetric methods, the co-polarized phase difference, its standard deviation, and complex correlation coefficient have been employed for slick detection [11], [13]. Finally, in compact-polarimetric algorithms, the parameters of wave entropy, polarization ratio and ellipticity, degree of polarization, complex correlation coefficient, and the conformity index have shown promise in oil spill detection [14], [15]. It should be finally noted that not all these open-water methods are directly applicable to sea ice infested environments as for example the idea of deviation from Bragg scattering is most noticeable in open water scenarios.

In terms of oil spills detection in sea ice environment, different remote sensing approaches have been previously considered. This includes the use of optical spectrometer images for oil spill mapping in winter through MODIS and Landsat images [16]. Another example of above-the-surface detection is presented in [17], where the reflectance of oil in different backgrounds was investigated to distinct the oil with sea water and sea ice. Moreover, a fluorescence polarization instrument has been developed in [18] for the detection of submerged oil spills relying on the property of viscous oil fractions exhibiting polarized fluorescence from beneath ice. Sonar technology has also been considered for oil detection provided having local access to beneath the ice [19].

In this paper, we will focus on above-the-surface approach, and within the microwave region. In particular, we utilize an active remote sensing approach in which the profile of interest is irradiated by microwaves. (Passive microwave radiometry has not been tested for oil spill detection in sea ice-infested waters [20]). In the microwave frequency regime, individual sensors attempt to detect oil in one particular scenario based on the oil presence within the profile (*i.e.*, above, encapsulated,

or beneath the sea ice). For instance, ground penetrating radar (GPR) has been effectively utilized to detect oil located between snow and sea ice, encapsulated between the ice layers, or below the sea ice utilizing a reflection-waveform inversion technique [21], [22]. Another developing technology is the frequency modulated continuous wave radar (FMCW) that has shown promise in the detection of oil near the surface of the sea ice [4]. More conventional radar technologies such as side looking airborne radar [23], and satellite SAR platforms [24] have been tested for oil detection in sea ice-covered waters based on signal strength and polarization ratios. It is reasonable to state that most of the oil spills in sea ice environment detection technologies are at a developing stage, and are recommended to be applied in conjunction with other sensors [4].

II. Problem Statement

This paper presents our multidisciplinary case study on the response of artificially-grown young sea ice to the introduction of crude oil via the water column beneath the sea ice. The aforementioned response includes the changes in (*i*) the single-polarization radar signature of the profile, and (*ii*) geophysical and chemical properties on a micro- and macro-scale. In particular, we are interested in studying the possibility of oil detection within the profile utilizing the radar data accompanied by prior information. To this end, we introduce a preliminary detection strategy, and interpret its retrieved results. The proposed detection strategy is based on a simplified electromagnetic inverse scattering formulation in which the effective complex permittivity of the profile, and subsequently the oil spill volume fraction thereof, are to be found from the measured radar data.

This paper is structured as follows. First, an overview of the experiment is given in Section III. Then in Section IV, the lidar measurements for surface roughness calculation are presented. The measured radar response of the system at a time interval of interest is brought in Section V. In Section VI, a scheme for "binary" (*i.e.*, presence or absence) oil detection utilizing such radar data is implemented. Finally in Section VII, the oil distribution within sea ice and the retrieval error for the effective volume fraction are investigated from a macro-level, micro-level, accompanied with *x*-ray and chemical analysis. This section is followed by a conclusion and recommendations in Section VIII.

III. Overview of the Experiment

The oil in sea ice experiment spanned from January to March in 2016 at the Sea-ice Environmental Research Facility (SERF), located at the University of Manitoba. The physical setting of the experiment consists of a specifically-designed open-ended tank of cylindrical shape, with a depth of about 1 m, and a radius of 1.5 m. This tank, shown in Figure 1, was filled with artificial sea-water having 32 salinity (herein, we refrain from using any unit for salinity), and the sea ice was allowed to grow under ambient temperature. This temperature during the period of interest in our experiment was approximately between -15 and -20 °C [25]. We were also able to heat the tank to melt the sea ice. Scaffolding facing this tank was used as a platform for the remote sensing equipment, as depicted in Figure 1.

Fig. 1. Scatterometer measures the normalized radar cross section (NRCS) of the oil-contaminated sea ice. In this figure, an external calibration is being performed utilizing a metallic trihedral.

This experiment was carried out in two phases. Phase one was a controlled experiment, and phase two was the experiment that is the focus of this paper. As will be seen, the controlled experiment was performed for data calibration and lidar characterization. In phase one, the ice was grown from open water to a thickness of about 30 cm. This sea ice was cored during its evolution, and its radar signature was also continuously measured. In phase two of the experiment, the sea ice was grown from the open water to a thickness of roughly 6 cm. A petroleum sour crude oil (from Tundra Oil and Gas Ltd.) was then introduced from beneath the sea ice at the center of the tank. The sea ice kept growing for a few weeks after this point through ice growth cycles. The radar signature of this evolving profile was measured temporally, and various cores were extracted during this phase across six equiphased radii.

IV. Lidar Scan of the Profile

Based on our previous remote sensing experiments at SERF, we found it to be useful to acquire lidar scans of the profile [26]. Not only did this provide us with the topography of the profile, but the analysis of data allows us to calculate the roughness parameters associated with the profile. In a simulation-based electromagnetic inversion approach for environmental parameter retrieval, having access to surface roughness data is helpful as it can provide the utilized inversion algorithm with a prior information. This prior information is particularly useful if we are limited in the number of measured data points. As will be seen in Section V, we will use this prior information in our proposed binary inversion algorithm.

To this end, on January 21st, a terrestrial laser scanner was used to acquire three-dimensional models of the snow and ice surface topography in the tank. Figure 2 depicts a scene of the profile's surfaces as captured through lidar. Two scans were acquired from this profile. The first one was taken of the snow surface (1 to 2 cm thick snow), and the second one from the

Fig. 2. A lidar scan of the profile's topography.

TABLE I
THE ROUGHNESS PARAMETERS CALCULATED BASED ON THE LIDAR SCANS ON 21ST OF JANUARY 2016. HEREIN, r_s, l_s, SD, AND ECC DENOTE THE RMS HEIGHT, CORRELATION LENGTH, STANDARD DEVIATION OF l_s, AND ECCENTRICITY OF THE ELLIPSE RESPECTIVELY.

Surface Type	r_s (cm)	l_s (cm)	SD	ECC
Snow	0.179	1.225	0.090	0.54
Sea Ice	0.390	0.965	0.088	0.81

sea ice surface after the snow was carefully removed from the sea ice surface.

Figure 3 depicts the topography of the area of interest produced utilizing the lidar data. The processing procedure as implemented in this paper to calculate the surface roughness parameters is explained below. First, the laser scanner data were pre-processed to (*i*) correct for the offset between scatterometer and laser scanner origin locations (required as the roughness parameters derived from the lidar data is to be used in conjunction with the data collected via the scatterometer), (*ii*) filter out anomalous laser returns from light blowing/falling snow, and (*iii*) crop the desired surface area for analysis (approximately a 2 m$\times$2 m square). Herein, our focus is to extract the snow and sea ice surface roughness parameters of root-mean-square height denoted by r_s, and correlation length denoted by l_s (These two parameter are the ones that will later be utilized in our inversion algorithm to simulate the NRCS data of a predicted profile.). To this end, we utilized the spectral decomposition and the two-dimensional autocorrelation length, following the algorithms brought in [27]. Next, the calculated parameters were corrected for inherent biases, principally involving the high inclination scanning angle, using a pre-established set of calibration functions [28].

The roughness parameters calculated through this methodology for the surface under investigation are reported in Table I. It is evident that the ice surface underlying the snow is relatively rough. Moreover, the snow surface was more isotropic than sea ice when considering the eccentricity (ECC) as reported in this table. An ECC value close to 0.5 means an isotropic, and an ECC value close to 1 means anisotropic surface distribution.

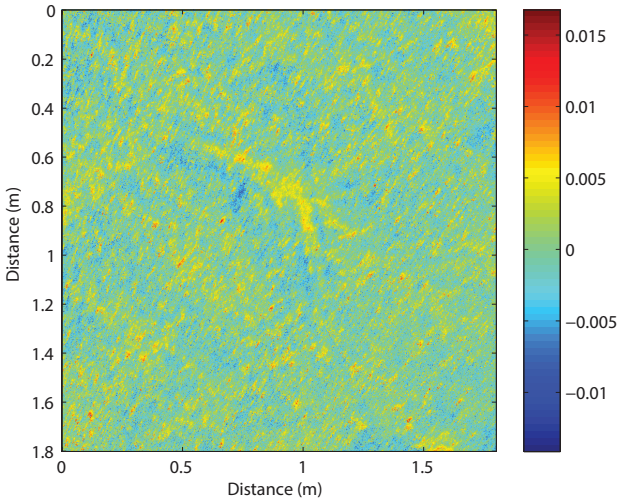

Fig. 3. The calculated surface topography (in meter) of the analyzed scene utilizing the lidar scans.

V. ELECTROMAGNETIC RESPONSE

In an inversion-based detection strategy, the response (output) of the domain under investigation (in our case, the sea ice profile) is often utilized and processed to infer some properties of that domain (*e.g.*, oil volume fraction, complex permittivity, etc.). Herein, the response to be used is an electromagnetic response, known as the normalized radar cross section (NRCS) data. To this end, we initially present the temporal NRCS data measured from the sea ice profile before and after contamination using a polarimetric scatterometer. Next, we investigate these data to assess the degree of its usefulness in the detection of oil presence, and possible retrieval of its volume fraction and amount. Finally, we look at the macro and micro-properties of the sea ice to put the retrieved information in perspective.

NRCS can be thought of as the radar signature of the illuminated profile. More precisely, the monostatic NRCS is related to the ratio of the power density of the scattered wave by the profile and that of the incident wave, and is defined as [29]

$$\sigma_{pq} \triangleq \frac{1}{C}\left\langle \lim_{R_r\to\infty}\left(4\pi R_r^2 \frac{S_s^p}{S_i^q}\right)\right\rangle \tag{1}$$

In (1), C is the surface area of our distributed target (*e.g.*, the sea ice surface illuminated by the antenna) located at a distance of R_r (its associated $limit$ denotes the far field condition). Also, S_i^q and S_s^p are the power densities of the illuminating and the scattered wave having a linear q and p polarization respectively. The symbol $\langle\ \rangle$ is defined as the ensemble average of a number of independent scans of the surface. This averaging accounts for the random scattering within the profile, and is achieved through averaging the azimuthly-measured NRCS values by our scatterometer. The central frequency of the utilized scatterometer is 5.5 GHz (in C-band), and the measurements are continuous in time.

A. NRCS Calibration

We utilized a metallic trihedral to externally calibrate our scatterometer measurements. The system also does a cold calibration in each scan. In addition, a so-called data calibration was also performed at a post-processing stage. This data calibration was deemed necessary since (*i*) tank was very close to the scatterometer, and we suspect that the sea ice profile might not be in the Fraunhofer far field region (although the radar system has an algorithm developed to partly alleviate this issue through the use of a correction defocusing factor [30]), and (*ii*) there are possible interferences and multiple reflections due to the small size of the tank that are not accounted for in our numerical model. For example, possible reflections at the edge of the tank are not modeled in our utilized forward electromagnetic scattering solver. Therefore, to alleviate the discrepancy between the actual wave propagation, and the modeled one, we utilize the following data calibration technique. This data calibration first compares the measured NRCS data for a known reference sea ice profile in the tank setting with the simulated NRCS data due to the same profile. This comparison will then result in a calibration factor that is the ratio of the simulated NRCS data to the measured one. This calibration factor will then be applied to subsequent NRCS measurements to create the calibrated measured NRCS data. In our experiment, this known reference sea ice profile was grown in a separate oil-free experiment (*i.e.*, phase one), and the true sea ice profile in this separate experiment was determined through physical sampling. We finally note that such a data calibration technique, often referred to as the scattered field data calibration, is also performed in microwave tomography applications [31] to reduce the so-called modeling error. This additional data calibration, estimated based on the comparison of the measured and simulated NRCS for a known sea ice profile in the tank setting, resulted in an equal shift in all temporal NRCS values. This reference sea ice profile was grown in a separate oil-free experiment, and the true profile was determined through physical sampling. It should be mentioned that data calibration is a necessary step in many cases of measured data processing [31].

B. NRCS Measurements

The NRCS was measured for various incidence angles, and at HH, VV, and HV/VH polarizations. After processing the raw data, the vertically- transmitted vertically-received NRCS (denoted by σ_{VV}) at the incidence angle of 57° was found to be the only suitable data to be used in our model. (Other measured data demonstrated unexpected jumps due to possible cable issues, experiment setup, size of the oil tank vs radar footprint at various incidence angles, etc.) This imposes a challenge on the choice of the oil detection algorithm, as many retrieval algorithms utilize dual- or quad-polarimetric data [8]. The calibrated σ_{VV} collected by the scatterometer at this incidence angle is depicted in Figure 4 for the period between February 8th at 7 pm to February 10th at 10 am. The significance of this time period is that it covers the pre-injection, during injection, and post-injection times within a few hours of stabilization. An interesting observation made in this figure is that the measured NRCS before and after the oil injection is relatively stable. But a drop of approximately 3.33 dB occurs as the result of injection. This information will be utilized in the upcoming Section VI for detection and retrieval. It should be finally noted that the air temperature during the oil injection settling time (*i.e.*, between the vertical lines in Figure 4) was almost constant at around -16.7$\pm$0.2°C.

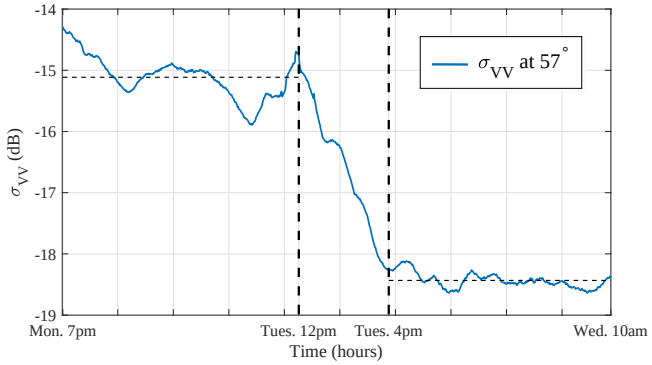

Fig. 4. The calibrated vertically-transmitted vertically-received NRCS (denoted by σ_{VV}) at 57° incidence angle from February 8th at 7 pm to 10th at 10 am, 2016. The horizontal dash lines indicate the average NRCS before and after the oil injection. The vertical dash lines bound the time span of oil settling in the tank.

(a) (b)

Fig. 5. Next few hours after the oil injection. (a) Oil patches within and below the sea ice are visible as darker areas. (b) Close-up shot of the sea ice surface. Oil has migrated upwards through the cracks or brine channels within the ice.

Finally, it should be mentioned that as the crude oil utilized in this experiment had relative low density and medium viscosity, we speculate that the oil moved up through the cracks or brine channels within the ice very quickly, as can be seen as dark spots in Figure 5 (the behavior of upward migration of oil in sea ice has also been investigated previously [32], [33]).

VI. Detection and Retrieval

In many detection scenarios, a radar image is produced from a scene with some of its pixels associated with a sub-scene of the oil-contaminated area. Depending on the nature of the collected measured data (*e.g.* coherent or incoherent, dual-, quad-, or compact-polarimetric, etc.), various parameters are

constructed for each pixel (*e.g.*, gray-scale threshold, entropy, etc.) [8]. Based on the distribution of such parameters, the pixels in the image associated with the oil spill are recognized. However, in our experiment in an oil tank with limited size, we have only a single measurement associated with the tank (*i.e.*, equivalent to a single pixel in a SAR image). Therefore, in our retrieval strategy, we have to trade the geographical distribution (*i.e.*, different pixels with or without oil at a single measurement time) with temporal distribution (*i.e.*, one pixel with and without oil at different measurement times). Moreover, we utilize a physical-based inversion algorithm to retrieve some information (complex permittivity) from the calibrated measured NRCS data. This usually means the use of an electromagnetic forward and inverse solvers. The forward solver simulates the NRCS associated with a known predicted profile, and the inverse solver retrieves the parameter(s) of interest via comparing the measured and simulated NRCS data. One reason for choosing this approach is that the inversion algorithm has access only to single polarization radar data (*i.e.*, σ_{VV}). Therefore, we cannot produce polarimetric parameters for oil detection similar to those in [8]. Finally, it should be noted that the physical-based approach has been previously implemented successfully to retrieve various snow-covered sea ice profiles [26], [34].

The first step in developing the retrieval model is to parametrize the profile under investigation. Based on our observations (and later samplings), the oil-contaminated sea ice profile in this experiment was highly heterogeneous on different scales. Therefore, we did not treat the injected oil as an individual layer within a multi-layered medium since it was distributed across the sea ice profile in various forms. Consequently, we decided to treat the profile as a rough half-space having a single effective complex permittivity value that represents this ensemble. (The half space consideration was based on the assumption that most of the incident power does not penetrate to the bottom of the ice at our frequency due to limited penetration [35], [36]). Moreover, the azimuth NRCS averaging which was performed by the scatterometer further justifies our decision, as it effectively considers a single averaged profile on the azimuth plane for each elevation incidence angle.

To simulate the NRCS associated with our model, an integral equation method is utilized as introduced in [29]. Considering the inverse solver, a Monte Carlo search method is utilized in which a minimum for an NRCS data misfit cost function is sought after. It should be noted that more complex inverse solvers were at hand, however the mentioned method is sufficient since (*i*) our forward solver has a trivial run-time, (*ii*) only one measured data point is available, and (*iii*) the unknown quantity in our proposed scheme will only be a single complex permittivity (in both pre- and post-injection stages).

It should be mentioned that we did not have access to new lidar scans for the scene under investigation. Nonetheless, we utilized the roughness parameters for sea ice as reported in Table I, as the experiment setting and the ice formation conditions are roughly similar to those of phase one (*i.e.*, controlled experiment used for calibration). Furthermore, average upper and lower bounds for the expected complex permittivity values for a typical young sea ice can be assumed based on dielectric measurements on similar ice types [35]. Such intentional bounding of our search spaces acts as a projection-based regularization scheme, and helps us to avoid local minima [37].

Before describing our proposed inversion strategy, as will be outlined in Section VI-A, let's consider the direct retrieval of the unknown parameters of the post-injection sea ice permittivity, and the effective volume fraction of oil utilizing the measured σ_{VV}. Our prior information is the oil complex permittivity value [38] and the roughness parameters. The inverse solver we utilized is the Differential Evolution (DE) [39]. This inverse solver is based on biological evolution, and iteratively minimizes our cost function so that the fittest element would survive into the next generation. The DE algorithm has been utilized for property retrieval of snow-covered sea ice before [34]. Herein, we used the DE algorithm to reconstruct the complex permittivity value as well as the oil spill volume fraction for the post-injection profile. The retrieved complex permittivity value is depicted in Figure 6 at four different runs for the exact same inversion problem. We also had 10 elements (*i.e.*, the searching members within one generation) and 10 generations (*i.e.*, the attempts to create a new set of elements with lower cost function values than the previous iteration) for each of the four separate runs. In this figure, the arrows show the movement of the elements during each generation towards the minimum. Also the amber line follows the best permittivity retrieved in every iteration. As can be seen, the algorithm cannot find the single global minimum of the problem as each scenario converges to a different complex permittivity. (We also observed this for the retrieved oil spill volume fraction.) This is most likely due to the imbalance between the number of unknown and known quantities. To handle this issue, the following inversion strategy is proposed and evaluated.

A. Inversion Strategy

Our proposed retrieval (inversion) strategy is as follows. First, the mean of the measured NRCS data (denoted by $\sigma_{VV}^{mean(meas)}$) for the period immediate before the oil injection is calculated. Next, the minimum of the following cost function for the range of the expected permittivity values at the frequency of operation is calculated,

$$CF(\epsilon) = \frac{|\sigma_{VV}^{mean(meas)} - \sigma_{VV}^{sim}(\epsilon)|^2}{|\sigma_{VV}^{mean(meas)}|^2} \tag{2}$$

In (2), σ_{VV}^{sim} denotes the simulated NRCS through our forward solver for a given predicted relative complex permittivity ϵ. Figure 7(a) depicts the logarithm of this cost function for the pre-injection period. The minimum in this figure corresponds to the relative complex permittivity of $5.2 + 1i$ for the sea ice in the pre-injection stage. (We are assuming a $e^{-i\omega t}$ time-dependency.) Next, a similar scheme is followed for the post-injection stage, with the cost function values (logarithmic scale) depicted in Figure 7(b) as a function of varying relative complex permittivity. The minimum in this figure corresponds to an effective relative complex permittivity of $3.2 + 0.6i$ for

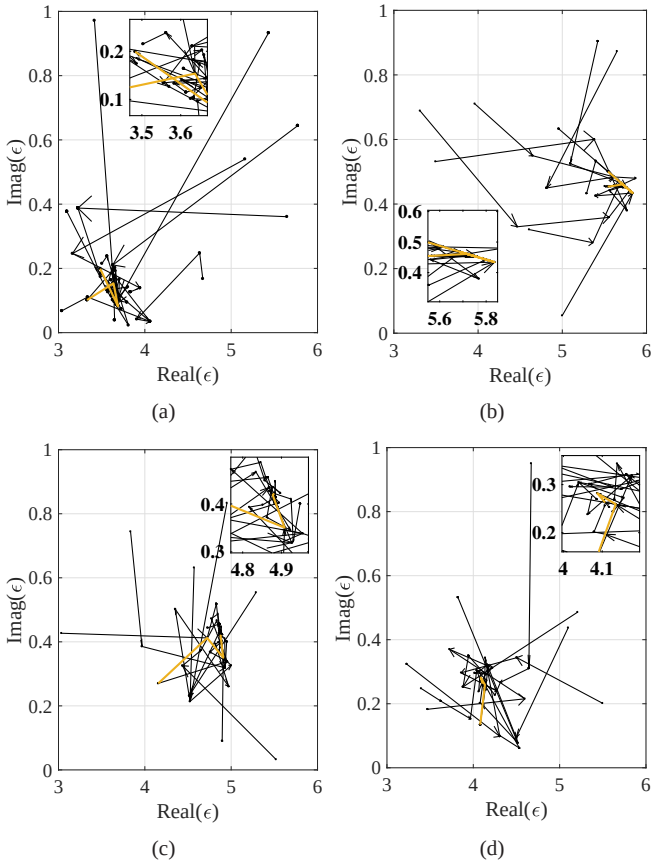

Fig. 6. Differential evolution inversion results for four independent runs for the exact same problem. Each arrow follows the path of an element during one generation. The amber line tracks the best retrieved dielectric. The box provides a magnified view of the final minimum found.

the post-injection profile. We have now retrieved the effective permittivity of the profile after and before oil injection.

Another prior information utilized in our approach is the oil complex permittivity. In practice, oil complex permittivity can be sampled and measured independently, and then be utilized as a known quantity in inversion algorithms dealing with the detection of that specific oil. It is also reported in the literature that once oil type is known, its permittivity can be estimated [4], [40]. (For example, in [41], the real part of the complex permittivity for oil is reported to vary between 2.2 to 2.3, and its imaginary part to vary between 0 to 0.02; similar results are also reported for light crude oil in [38].) Although there is a large variety of oil types and densities, and weathering and aging conditions might change the oil's permittivity, this is not within the scope of this paper. Therefore, we assume to know the complex permittivity of oil, which is taken to be $2.2 + 0.05i$.

Now if we consider that the sea ice permittivity has not changed after oil injection, the following simplified formulation is utilized for the calculation of the effective volume fraction of the oil as the true heterogeneous distribution of the oil within the profile is unknown [42],

$$\upsilon_{oil} = \frac{|(\epsilon_{eff} - \epsilon)(\epsilon_s + 2\epsilon)|}{|(\epsilon_s - \epsilon)(\epsilon_{eff} + 2\epsilon)|} \tag{3}$$

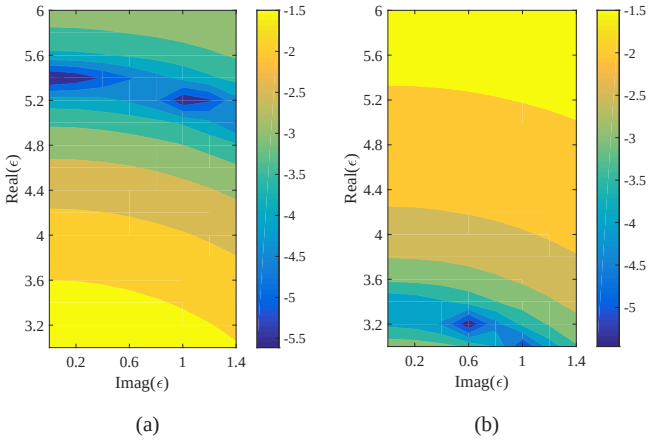

Fig. 7. Logarithm contour plot of the cost function value for (a) pre-oil injection, and (b) post-oil injection.

TABLE II
RETRIEVED PARAMETERS THROUGH THE UTILIZED INVERSION SCHEME. ϵ_{eff} DENOTES THE PROFILE'S DIELECTRIC AFTER OIL INJECTION.

$\epsilon_{sea\ ice}$	ϵ_{eff}	υ_{oil}
5.2+1i	3.2+0.6i	0.5976

In (3), υ_{oil} denotes the effective oil volume fraction. Also ϵ_{eff}, ϵ_s, and ϵ denote the effective permittivity of the profile after oil injection, the oil permittivity, and the sea ice permittivity receptively. Based on (3), the volume fraction of the introduced oil is estimated to be 0.5976. The retrieved parameter values are reported in Table II.

The retrieved value for the effective oil volume fraction, υ_{oil}, is large enough that would trigger a warning after an spill has occurred. Therefore, this strategy seems promising to be considered in a future spill detection approach in conjunction with other sensors [4]. Also, due to its simplicity and computational efficiency, it has the potential to be used on the fly so as to cover large areas. We finally note that the retrieved volume fraction was larger than the expected value; roughly 7 times if we neglect the actual oil distribution pattern within the profile. This deviation is explained in the next section.

VII. Analysis of the Retrieval Accuracy

It is clear that there is an inherent error associated with simplifying the profile that allowed us to use a practical retrieval strategy. But apart from this source of error, the large retrieved value for the volume fraction can be interpreted as an indication that the incidence waves have interrogated a heavily-effected part of the sea ice. Considering the limited penetration depth of interrogating microwaves, it can be concluded that the interrogating microwaves "see" the top portion of the oil-contaminated sea ice profile more effectively. Due to this, it is expected that the inversion algorithm is biased (or, more sensitive) toward the top portion of the oil-contaminated sea ice. That being said, and noting the high value for the retrieved oil spill volume fraction, it can be concluded that a large amount of oil could exist close to the surface of the

(a)

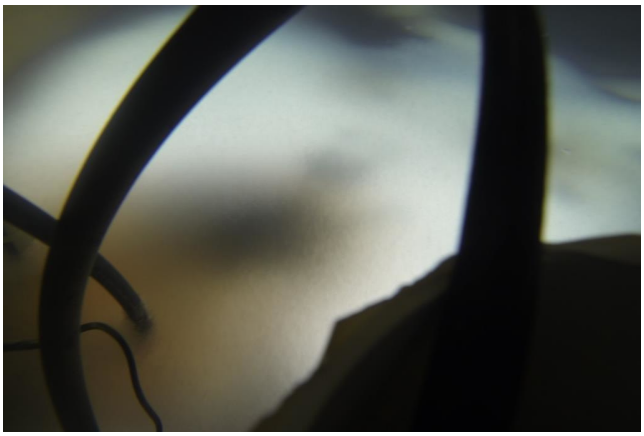

(b)

Fig. 8. The surfacing of oil on the sea ice in the latter stages of the experiment. (a) Above photo taken at 10 am February 11th. (b) Beneath sea ice photo taken from within the water at 11 am February 12th. In this photo, the black section on the bottom right is the observation tube.

profile. In what follows, we present the physical evidence supporting the speculation of having a larger amount of oil spills close to the sea ice surface.

After the oil was introduced in the water column beneath the sea ice, it moved up within the tank, and partly replaced the highly dielectric saline water at the porous soft end of the ice and then migrated up to the surface. This speculation is partly supported when we look at Figure 8. Only by 11th of February at 10 am, a significant amount of oil has surfaced on the sea ice, as evident in Figure 8(a). Moreover, an under ice photo on the 12th of February at 11am shows that there is no oil left underneath the profile. Most of the large dark spots seen in this photo, Figure 8(b), are the shadows corresponding to the surfaced oil. In the meanwhile, it should be taken into consideration that not all the surfaced oil moved up through the ice cracks or the brine channels, as a portion of oil leaked towards the surface through the gap between the sea ice and the tank interface due to an undesired flaw in the tank's design.

Another reason behind the larger than expected retrieved volume fraction for the injected oil can be traced back to the speculation of expedited brine rejection as oil moved up

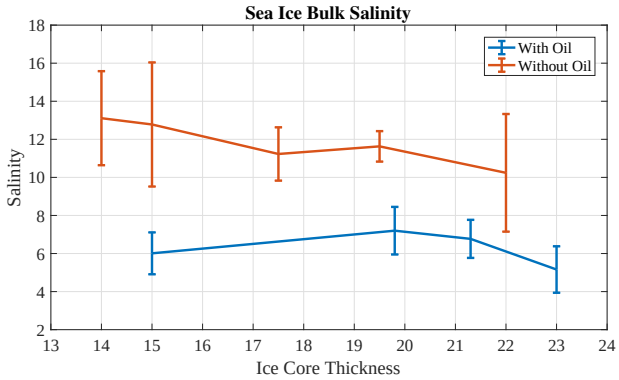

Fig. 9. Sea ice salinity comparison in the presence and absence of oil.

through the sea ice cracks and channels. Such desalinization leads to a lower permittivity for sea ice, as brine has a very high permittivity of about $48 + 44i$ at the experiment's temperature [43]. In other words, the reduction of the effective permittivity of the entire profile after oil injection, is not only due to the direct presence of the oil (having a lower permittivity than the original sea ice), but also the reduction of the sea ice permittivity as the background material for the post injection mixing formula. Since the amount of brine loss is not known before any in-situ sampling, it cannot be accounted for in the renewed permittivity of the background sea ice utilized in (3). The evidence indicating to such desalinization and the oil migration through the sea ice comes from the (*i*) macro-level, (*ii*) micro-level, and (*ii*) chemical analysis of the contaminated oil physical samples extracted from the tank. In what follows, these three investigations are presented.

A. Macro-level Analysis

On a macro-level, the bulk salinity of some of the extracted cores having similar age and core thicknesses between phase one (no oil present) and phase two (pertaining oil injection) is presented in Figure 9. When plotting this figure, the ice cores are sectionized as top, middle, and bottom. The error bars represent the salinity standard deviation in each of the cores for their associated three sections. The open water in both cases had the same salinity of 32, and the growth condition and settings for both phases are similar. Nonetheless, on average the non-contaminated sea ice is 55% more saline than the contaminated sea ice for the extracted cores. This reduction in salinity is significant. These cores were extracted on the 1st of March, when oil had ample time to move through the sea ice. This phenomenon is expected to have similarly lowered the salinity of the sea ice at the early stages after the oil injection, but on a lower scale. This can contribute to the reduction of the measured NRCS as shown in Figure 4. As a further comparison, the salinity values for ice cores in phase two were compared to cores with similar thickness values extracted in a separate experiment carried out at the main SERF pool in 2015. The salinity of phase two cores were still consistently lower than those extracted in SERF 2015. (Both experiments had the same open water salinity.)

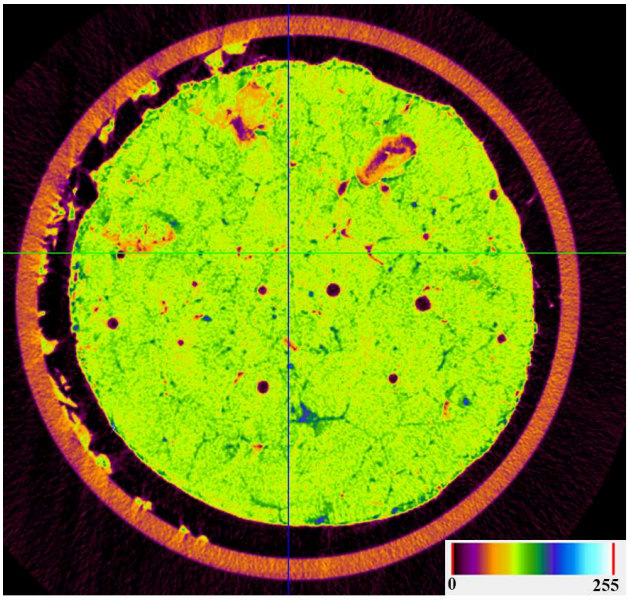

Fig. 10. The *x*-ray of an oil-contaminated sample. Air, oil, ice, and brine are represented by black (color range 2-72), orange (color range 105-136), green (color range 137-170), and blue (color range 171-252) respectively.

B. Micro-level Analysis

X-ray computed tomography (CT) has been previously utilized for sea ice micro-structure and component analysis [44]. Herein, we utilized a CT *x*-ray SkyScan 1174 Bruker system to investigate the micro-structure of an oil-contaminated sea ice sample. To this end, a sample was carefully collected from the interior of a large ice core extracted in February 2016, and analyzed by our *x*-ray machine. (Large cores themselves cannot be placed inside this *x*-ray system.) The sample was cylindrical with 3 cm radius and 2.5 cm height. This sample was placed in a polypropylene tube when being analyzed inside the CT scanner. Our analysis is based on creating three-dimensional images of the sample's density contrast. Data processing for the *x*-ray includes removal of the ring artifacts, and application of a box Gaussian smoothing.

Figure 10 depicts a cross-section slice of our sample. The ice, brine, air, and oil can be distinguished due to their different *x*-ray attenuation characteristics and the range of intensities. This figure is colored coded based on histogram values (ranging from 0 to 255) so that each component can be visually distinguished, with ice as green (color range 137-170), brine as blue (color range 171-252), air as black (color range 2-72), and oil as orange (color range 105-136). If investigated closely, we notice the following two items. (*i*) A portion of the oil seems to have been spread across the core in minute pockets. These may have been inhabited with brine once, but pushed out as the oil moved up. (*ii*) A large amount of oil seems to have gathered around the empty spaces within the sample (*e.g.*, the cracks or the air inclusions). To better visualize this, a three-dimensional image from a section of the sample is brought in Figure 11. In this visualization, only the air (presented in white and mostly seen as spheres in this figure), and the oil (presented in red) are represented. As can

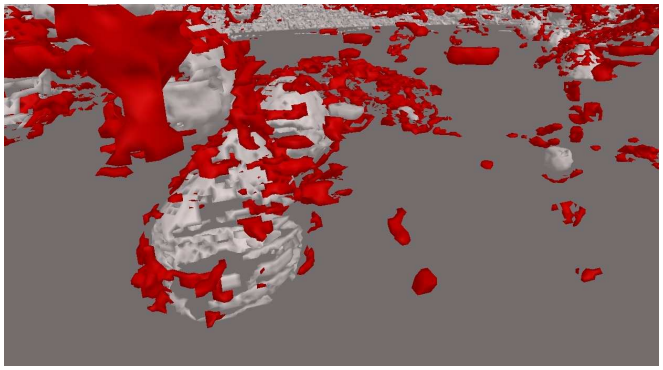

Fig. 11. Three-dimensional visualization of the oil (red) and air (white) in the sample under investigation. The average bubble area is about $2.8 \times 10^{-2}\ mm^2$.

be seen, although there are various red spots suspended in the background (oil in the ice), there seem to be a tendency for oil and air bubbles to converge. It should be noted that this does not necessarily contradict the idea of dielectric reduction after oil injection. The dielectric contrast of oil to air is 2:1, while for oil to brine is 1:20. Therefore, even if the oil has a tendency to gravitate toward air bubbles in this sample, a small brine rejection can still reduce the effective dielectric value significantly.

Finally, we acknowledge that drawing a general conclusion based on a single sample analyzed in this section is not recommended. It is possible that different samples at various depths of the core, various stages of the sea ice growth, and different oil volume fractions might result in a different micro-structure. Moreover, linking the micro-structure to the dielectric value that is calculated based on macro-properties (*e.g.*, bulk salinity of the sample) is not straightforward. Nonetheless, this example demonstrated a plausible micro-level scenario for our case study, and provided us with some insight into the possible behavior of the oil in sea ice.

C. Chemical Analysis

In this section, we study the effect of oil introduction to the sea ice from a chemical perspective. To this end, we consider two different properties: (*i*) oil concentration, and (*ii*) oil composition at different depths of the oil-contaminated sea ice. These properties have been previously studied for various oil-contaminated sea ice types [45], [46]. Our chemical analysis helps us to investigate the oil partitioning in the oil-contaminated sea ice cores collected during our experiment. For current analysis, we had access to three ice core samples collected from different locations across the pool, and at different points of the sea ice evolution.

Extraction, cleanup, and chemical analysis of individual ice core sections are described briefly below. The crude oil was separated from the salt water using glass separatory funnels and hexane. The collected oil fractions were then concentrated by fully reducing the solvent to dryness with the use of rotory and nitrogen evaporization. The oil volume for each respective ice core section was measured volumetrically, and their masses were measured with the use of analytical balance. Volumes

TABLE III
MEASURED OIL VOLUMES, DENOTED BY V^{oil} IN MILLILITER, FOR THE TOP (0-2.5 CM), MIDDLE (2.5 CM-7.5 CM), AND BOTTOM (7.5 CM-REST) SECTIONS FOR THREE ICE CORES EXTRACTED AT FEB. 12TH, FEB. 18TH, AND MARCH 1ST 2016.

Date	V^{oil}_{top} (mL)	V^{oil}_{middle} (mL)	V^{oil}_{bottom} (mL)
Feb. 12th	7.3	1.4	0.4
Feb. 18th	12.3	3.4	2.3
March 1st	1.3	0.3	0.24

for the top (*i.e.*, pertaining air-ice interface), middle, and bottom (*i.e.*, pertaining ice-water interface) sections of these cores are reported in Table III. Based on the ever-increasing volumes of the oil from the bottom to the top sections in all three cores, it can be concluded that the oil has moved upwards through brine channels and any accessible cracks after its introduction from beneath the sea ice. This observation further supports our justification for the large retrieved value of the effective volume fraction of oil, υ_{oil}.

Furthermore, the variation of oil volumes from one core to another is a good indication of the oil distribution heterogeneity, as noted before. It should be noted that the oil volume in the top section of the core collected on 1st of March is considerably lower compared to the cores collected in February. Apart from the possible link to physical heterogeneity of oil distribution across the pool, the sea ice was covered by an average 1.5 cm snow for a number of days at this stage. Consequently, snow soaked the oil at its basal layer, and this possibly contributed to a lower oil volume at the ice top.

Moreover, the individual oil samples were diluted with hexane, and analyzed by a Leco Pegasus 4D GC×GC-HR-TOF-MS. The result of our analysis for the top, middle, and bottom sections of the sample extracted on February 18th is depicted in Figure 12. The chromatographic profiles for each of the three ice core sections appeared for the most part to be identical. We speculate that the similarity between profiles can likely be attributed to the fast surfacing of the oil through sea ice cracks and brine channels. Furthermore, the hydrocarbon composition of the technical oil mixture was determined using a GC-MS method (Agilent 7890A). Thus, the estimates for the relative percentages of major compound classes (*i.e.*, Alkanes, Naphthenes, and Aromatics) have been calculated with respect to their relative areas provided by the GC chromatogram. These values are reported in Table IV. Moreover, the amounts for notable minor compounds of BTX and Hydrogen Sulphide (H2S) are provided by the oil company. These include Toluene 100 ppm, Xylene 100 ppm, Benzene 10 ppm, Hydrogen sulphide 10 ppm. We also identified small quantities of Sulphur and Nitrogen Compounds. Based on the dominance of the relative percent of alkanes in the mixture, the oil can be characterized as light crude oil. Also the crude oil contains residual amounts of sulphur that is characteristic of its sour nature.

TABLE IV
CHEMICAL COMPOSITION OF TUNDRA CRUDE OIL UNDER INVESTIGATION.

Composition	Alkanes	Naphthenes	Aromatics
Relative (%)	72.1	17.8	10.1

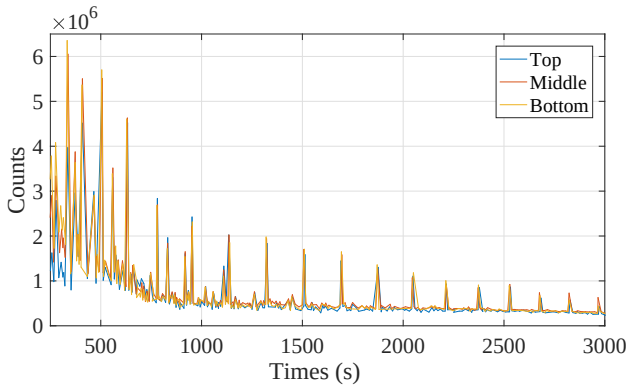

Fig. 12. Total ion chromatograms of the top, middle, and bottom sections of the oil-contaminated sea ice sample extracted on February 18th 2016.

VIII. CONCLUSION AND FURTHER DISCUSSION

In the winter of 2016, an experiment on crude oil injection in young sea ice was carried out at SERF, University of Manitoba. In this paper, we presented some of our multidisciplinary findings regarding the impact of this oil injection in our controlled sea ice environment. It was shown that the binary detection of oil through the measured NRCS data in this experiment was possible via retrieving the oil spill volume fraction. This retrieved volume fraction has the potential to be utilized as an auxiliary way to estimate the amount of the spilled oil, knowing the sea ice thickness in the area, and the radar footprint at which the drop in the NRCS value was observed.

One reason that our retrieval accuracy suffered in this experiment was the excessive surfacing of the oil, which was partly due to our experimental setup. In addition to different simplifications in our electromagnetic forward solver, the other modeling error in our algorithm was to consider the changes in the complex permittivity of sea ice to be negligible after the oil injection. This problem can be dealt with through considering the post-injection sea ice permittivity as an extra unknown in the inversion algorithm. This, however, requires having access to more measured data points from the oil-contaminated sea ice in various incidence angles and/or polarizations. Moreover, having access to more data reduces our need to utilize prior information. In general, it is recommended to have platforms with multiple sensors on-board when considering an operational system. One strong benefit of having a multi-sensor system would be to help relate the cause of NRCS drop to the change of ice type, or the presence of oil.

Furthermore, this paper was mainly focused on the time period around the introduction of the oil. But this temporal experiment offered other interesting cases to be studied in future. One example is the investigation of the geophysical changes to the oil-contaminated sea ice profile due to oil thermal properties. Also, if the oil surfaces, its albedo contrast with respect to the background, and/or the possible formation of melt ponds due to heat absorption can be utilized for

oil spill detection by active or passive systems. Last but not least, it is always useful to increase the information content of the measured data and use more sophisticated inversion algorithms. For example, instead of single polarization NRCS data used in this paper, one can measure and use dual-, quad-, or compact-polarimetric data so as to have access to more information about the region of interest.

ACKNOWLEDGMENT

We would like to acknowledge the SERF technician David Binne, and David Babb for their assistance in the preparations of the experiment. Furthermore, we acknowledge the financial contributions of the University of Manitobas GETS program, the Natural Sciences and Engineering Research Council of Canada, the Canada Excellence Research Chair program, and the Canada Research Chair program. This paper is also a contribution to the Arctic Science Partnership (ASP) program and ArcticNet.

REFERENCES

[1] T. Stocker, D. Qin, G. Plattner, M. Tignor, S. Allen, J. Boschung, A. Nauels, Y. Xia, V. Bex, and P. Midgley, *Climate Change 2013: The Physical Science Basis. Contribution of Working Group I to the Fifth Assessment Report of the Intergovernmental Panel on Climate Change*. Cambridge University Press, 2013.

[2] L. Smith and S. Stephenson, "New Trans-Arctic shipping routes navigable by midcentury," *Proceedings of the National Academy of Sciences*, vol. 110, no. 13, pp. E1191–E1195, 2013.

[3] Memorial University of Newfoundland and Centre for Cold Ocean Resources Engineering, "Microwave systems for detecting oil slicks in ice-infested waters : phases II and III," Environmental Protection Service, Tech. Rep., 1980.

[4] W. S. Pegau, J. Garron, and L. Zabilansky, "Detection of oil on-in-and-under ice - final report 5.3," Arctic Response Technology, Tech. Rep., 2016.

[5] K. Lee, M. Boufadel, B. Chen, J. Foght, P. Hodson, S. Swanson, and A. Venosa, "The behaviour and environmental impacts of crude oil released into aqueous environments," The Royal Society of Canada Expert Panel, Tech. Rep., 2015.

[6] M. Fingas and C. Brown, "Review of oil spill remote sensing," *Marine Pollution Bulletin*, vol. 83, no. 1, pp. 9 – 23, 2014.

[7] A. H. S. Solberg, "Remote sensing of ocean oil-spill pollution," *Proceedings of the IEEE*, vol. 100, no. 10, pp. 2931–2945, Oct 2012.

[8] M. Migliaccio, F. Nunziata, and A. Buono, "SAR polarimetry for sea oil slick observation," *International Journal of Remote Sensing*, vol. 36, no. 12, pp. 3243–3273, 2015.

[9] F. Nunziata, A. Gambardella, and M. Migliaccio, "On the degree of polarization for SAR sea oil slick observation," *ISPRS Journal of Photogrammetry and Remote Sensing*, vol. 78, pp. 41 – 49, 2013.

[10] M. Migliaccio, F. Nunziata, A. Montuori, and C. Brown, "Marine added-value products using radarsat-2 fine quad-polarization," *Canadian Journal of Remote Sensing*, vol. 37, no. 5, pp. 443–451, 2012.

[11] S. Skrunes, C. Brekke, and T. Eltoft, "Characterization of marine surface slicks by radarsat-2 multipolarization features," *IEEE Transactions on Geoscience and Remote Sensing*, vol. 52, no. 9, pp. 5302–5319, Sept 2014.

[12] M. Migliaccio and F. Nunziata, "On the exploitation of polarimetric SAR data to map damping properties of the Deepwater Horizon oil spill," *International Journal of Remote Sensing*, vol. 35, no. 10, pp. 3499–3519, 2014.

[13] F. Nunziata, A. Gambardella, and M. Migliaccio, "A unitary mueller-based view of polarimetric SAR oil slick observation," *International Journal of Remote Sensing*, vol. 33, no. 20, pp. 6403–6425, 2012.

[14] A. B. Salberg, O. Rudjord, and A. H. S. Solberg, "Oil spill detection in hybrid-polarimetric SAR images," *IEEE Transactions on Geoscience and Remote Sensing*, vol. 52, no. 10, pp. 6521–6533, Oct 2014.

[15] F. Nunziata, M. Migliaccio, and X. Li, "Sea oil slick observation using hybrid-polarity SAR architecture," *IEEE Journal of Oceanic Engineering*, vol. 40, no. 2, pp. 426–440, April 2015.

[16] J. Praks, M. Eskelinen, J. Pulliainen, T. Pyhalahti, and M. Hallikainen, "Detection of oil pollution on sea ice with airborne and spaceborne spectrometer," in *IGARSS 2004. 2004 IEEE International Geoscience and Remote Sensing Symposium*, vol. 1, Sept 2004, p. 276.

[17] B. Liu, W. h. Zhu, and Y. Li, "Spectral characteristics analysis of oil film among sea ice," in *2015 IEEE International Geoscience and Remote Sensing Symposium (IGARSS)*, July 2015, pp. 3450–3453.

[18] J. Bello, A. Smirnov, and P. Toomey, "Development of a fluorescence polarization submersible instrument for the detection of submerged heavy oil spills," *Proceedings of Ocean Sensing and Monitoring IV*, vol. 8372, pp. WA59–WA70, 2012.

[19] J. Wilkinson, T. Boyd, B. Hagen, T. Maksym, S. Pegau, C. Roman, H. Singh, and L. Zabilansky, "Detection and quantification of oil under sea ice: The view from below," *Cold Regions Science and Technology*, vol. 109, pp. 9 – 17, 2015.

[20] T. Puestow, L. Parsons, I. Zakharov, N. Cater, P. Bobby, M. Fuglem, G. Parr, A. Jayasiri, S. Warren, and G. Warbanski, "Oil spill detection and mapping in low visibility and ice: Surface remote sensing," Arctic Response Technology, Tech. Rep., 2013.

[21] J. H. Bradford, E. L. Babcock, H.-P. Marshall, and D. F. Dickins, "Targeted reflection-waveform inversion of experimental ground-penetrating radar data for quantification of oil spills under sea ice," *GEOPHYSICS*, vol. 81, no. 1, pp. WA59–WA70, 2016.

[22] J. H. Bradford, D. F. Dickins, and P. J. Brandvik, "Assessing the potential to detect oil spills in and under snow using airborne ground-penetrating radar," *GEOPHYSICS*, vol. 75, no. 2, pp. G1–G12, 2010.

[23] D. Dickins and J. Andersen, "Evaluation of airborne remote sensing systems for oil in ice detection," SINTEF Materials and Chemistry-Report no. 28, Tech. Rep., 2010.

[24] C. Brekke, B. Holt, C. Jones, and S. Skrunes, "Discrimination of oil spills from newly formed sea ice by synthetic aperture radar," *Remote Sensing of Environment*, vol. 145, pp. 1 – 14, 2014.

[25] "Historical data," http://climate.weather.gc.ca/, WINNIPEG INTL A.

[26] N. Firoozy, A. S. Komarov, P. Mojabi, D. G. Barber, J. C. Landy, and R. K. Scharien, "Retrieval of young snow-covered sea-ice temperature and salinity evolution through radar cross-section inversion," *IEEE J. Ocean. Eng.*, vol. 41, no. 2, pp. 326–338, April 2016.

[27] J. Landy, D. Isleifson, A. Komarov, and D. Barber, "Parameterization of centimeter-scale sea ice surface roughness using terrestrial lidar," *IEEE Trans. Geosci. Remote Sens.*, vol. 53, no. 3, pp. 1271–1286, March 2015.

[28] J. C. Landy, A. S. Komarov, and D. G. Barber, "Numerical and experimental evaluation of terrestrial lidar for parameterizing centimeter-scale sea ice surface roughness," *IEEE Transactions on Geoscience and Remote Sensing*, vol. 53, no. 9, pp. 4887–4898, Sept 2015.

[29] F. T. Ulaby and D. G. Long, *Microwave Radar and Radiometric Remote Sensing*. University of Michigan Press, 2014.

[30] Radar Calibration Team, "C-band polarimetric scatterometer data system software - revision D, including polarimetric calibration and near field correction analysis," ProSensing Inc., Tech. Rep., 2004.

[31] M. Ostadrahimi, P. Mojabi, C. Gilmore, A. Zakaria, S. Noghanian, S. Pistorius, and J. LoVetri, "Analysis of incident field modeling and incident/scattered field calibration techniques in microwave tomography," *IEEE Antennas Wireless Propag. Lett.*, vol. 10, pp. 900–903, 2011.

[32] E. Lewis, "Oil in sea ice - pacific marine science report 78-12," Institute of Ocean Sciences, Patricia Bay, Tech. Rep., 1976.

[33] M. Fingas and B. Hollebone, "Review of behaviour of oil in freezing environments," *Marine Pollution Bulletin*, vol. 47, no. 912, pp. 333 – 340, 2003.

[34] N. Firoozy, P. Mojabi, J. Landy, and D. G. Barber, "Landfast first-year snow-covered sea ice reconstruction via electromagnetic inversion," *IEEE Journal of Selected Topics in Applied Earth Observations and Remote Sensing*, vol. 9, no. 6, pp. 2414–2428, June 2016.

[35] M. Shokr and N. Sinha, *Sea Ice Physics and Remote Sensing*. John Wiley & Sons Inc, 2015, ch. 3, pp. 99–137.

[36] C. A. Balanis, *Advanced Engineering Electromagnetics*. Wiley-IEEE Press, 1989, ch. 4, pp. 149–150.

[37] P. Mojabi and J. LoVetri, "Overview and classification of some regularization techniques for the Gauss-Newton inversion method applied to inverse scattering problems," *IEEE Trans. Antennas Propag.*, vol. 57, no. 9, pp. 2658–2665, 2009.

[38] T. Friiso, Y. Schildberg, O. Rambeau, T. Tjomsland, H. Fordedal, and J. Sjoblom, "Complex permittivity of crude oils and solutions of heavy crude oil fractions," *Journal of Dispersion Science and Technology*, vol. 19, no. 1, pp. 93–126, 1998.

[39] P. Rocca, G. Oliveri, and A. Massa, "Differential evolution as applied to electromagnetics," *Antennas and Propagation Magazine, IEEE*, vol. 53, no. 1, pp. 38–49, 2011.

[40] B. Minchew, C. E. Jones, and B. Holt, "Polarimetric analysis of backscatter from the Deepwater Horizon oil spill using L-band synthetic aperture radar," *IEEE Transactions on Geoscience and Remote Sensing*, vol. 50, no. 10, pp. 3812–3830, Oct 2012.
[41] C. Brekke, B. Holt, C. Jones, and S. Skrunes, "Towards oil slick monitoring in the arctic environment," *6th International Workshop on Science and Applications of SAR Polarimetry and Polarimetric Interferometry*, August 2013.
[42] A. Sihvola and J.-A. Kong, "Effective permittivity of dielectric mixtures," *IEEE Trans. Geosci. Remote Sens.*, vol. 26, pp. 420–429, 1988.
[43] A. Stogryn and G. Desargant, "The dielectric properties of brine in sea ice at microwave frequencies," *IEEE Trans. Antennas Propag.*, vol. 33, no. 5, pp. 523–532, 1985.
[44] O. Crabeck, R. Galley, B. Delille, B. Else, N. Geilfus, M. Lemes, M. Des Roches, P. Francus, J. Tison, and S. Rysgaard, "Imaging air volume fraction in sea ice using non-destructive x-ray tomography," *The Cryosphere*, vol. 10, no. 3, pp. 1125–1145, 2016.
[45] I. A. Nemirovskaya, "Hydrocarbons in the snow-ice cover of different areas of the white sea," *Oceanology*, vol. 54, no. 3, pp. 298–307, 2014.
[46] Z. Wang and M. F. Fingas, "Development of oil hydrocarbon fingerprinting and identification techniques," *Marine Pollution Bulletin*, vol. 47, no. 912, pp. 423 – 452, 2003.

Nariman Firoozy (M'11) received his PhD in electrical engineering in collaboration with the Centre for Earth Observation Science from the University of Manitoba in 2016 on the topic of snow-covered sea ice remote sensing. Dr. Firoozy is currently a Postdoctoral Fellow at the University of Manitoba, and also the remote sensing lead on oil spill detection at the Sea-ice Environmental Research Facility. Dr. Firoozy is interested in research topics in the areas of applied electromagnetics, and remote sensing of the environment. He also has considerable research fieldwork experience in those areas. Dr. Firoozy is the founder and chair of the IEEE GRS-AES Winnipeg Chapter.

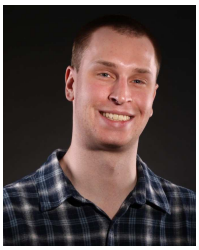

Thomas Neusitzer (S'14) received his BSc (with Distinction) in electrical engineering from the University of Manitoba in 2015. He is currently an electrical engineering MSc student with the University of Manitoba. His research interests include electromagnetics, microwave remote sensing of sea ice and its applications in Arctic oil spill detection. Mr. Neusitzer is a recipient of the Natural Sciences and Engineering Research Council Alexander Graham Bell Canada Graduate Scholarship, the A. Keith Dixon Graduate Scholarship in Engineering, and the Manitoba Hydro Undergraduate Thesis Prize in electrical engineering.

Tyler Tiede received his BSc degree in electrical engineering in 2014 from the University of Manitoba. Currently, he is pursuing his MSc degree in electrical engineering with the collaboration with the Centre for Earth Observation Science at the University of Manitoba. He has received various awards including the University of Manitoba Graduate Fellowship and Manitoba Graduate Scholarship. Tyler's research interests include active microwave remote sensing, antenna design, and machine learning.

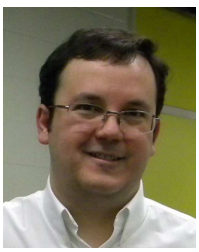

Marcos J. L. Lemes received his PhD degree from the University of Manitoba in 2010. He worked on several projects in Chemical and Environmental Technology Department at Institute of Energy and Nuclear Research (Ipen), Sao Paulo, Brazil, from 1987 to 2003. From 2010 to 2012, he was a Postdoctoral Research Fellow at Department of Chemistry and Environment and Geography, University of Manitoba. Currently, he is a Research Associate in Centre for Earth Observation Science at CHR Faculty of Environment, Earth and Resources, University of Manitoba, working on climate change research topics.

Jack Landy received BSc and MSc Res. degrees from the University of Durham, U.K., in 2009 and 2011, specializing in airborne LiDAR remote sensing. He received his PhD degree from the University of Manitoba, Canada, in 2016, specializing in sea ice geophysics and remote sensing. He is currently Lecturer of Geodesy at the Glaciology Centre, University of Bristol, U.K., researching the physical properties of Arctic sea ice during the summer melt season using satellite remote sensing techniques including altimetry and polarimetric imaging radar.

Puyan Mojabi is an Assistant Professor in the department of electrical and computer engineering at the University of Manitoba. He served as the National Representative of Commission E on the Canadian National Committee of URSI (2013-2015), and the Chair of the IEEE Winnipeg Section (2015). In 2017, Dr. Mojabi received the University of Manitobas Falconer Emerging Researcher Rh Award for Outstanding Contributions to Scholarship and Research in the Applied Sciences category. He also received three URSIs Young Scientist Awards in 2014, 2015, and 2016, as well as the 2013-2014 Excellence in Teaching Award from the Faculty of Engineering at the University of Manitoba.

Søren Rysgaard is a professor and Canada Excellence Research Chair in Arctic geomicrobiology and climate change. His research interests include marine microbiology and biogeochemistry in Arctic sea ice, and understanding the carbon and nutrient cycling in Arctic marine ecosystems. He is also a scientific leader with the Arctic Science Partnership, founding Director of Greenland Climate Research Centre (Greenland), and Arctic Research Centre (Denmark). Dr. Rysgaard has led several science projects in the Arctic (NOG, CAMP, Anoxia, Sea Ice dynamics, FreshLink, GCRC) and initiated two marine monitoring programs (High- and Sub-arctic). He has also authored/co-authored 175 publications.

Gary Stern received his PhD in chemistry on mass spectrometry from University of Manitoba in 1991. He is currently a Professor at the University of Manitoba, Centre for Earth Observations Sciences. For the past 25 years his research has involved the study of environmental pathways of contaminants in Arctic marine and freshwater ecosystems. More recently his work has focused in on the development of oil detection and remediation technologies, impacts and fate of oil spills in Arctic marine environments. Dr. Stern is currently the co-lead of the GENICE project that involves genomics research in oil spill preparedness and emergency response in an Arctic marine environment.

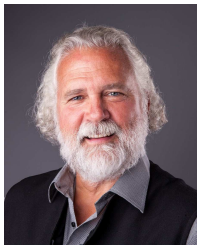

David G. Barber received his PhD degree from the University of Waterloo in 1992. He has been a professor at the University of Manitoba since 1993 and received a Canada Research Chair in Arctic System Science in 2002. He has published over 240 articles and has been scientific leader in large network programs (NOW, CASES, ArcticNet, CFL, BaySys and CMO). He is an invited member of several national (NSERC GSC 09; NSERC IPY, NSERC Northern Supplements) and international (GEWEX, IAPP, CNC-SCOR, IARC) committees. Dr Barber is a fellow of the Royal Society of Canada (Science Academy), an Officer of the Order of Canada, and a UM Distinguished Professor.

Durell S. Desmond received his BSc in physical chemistry from the University of Manitoba in 2015. He is currently an MSc student with the Centre for Earth Observation Science at the University of Manitoba, Winnipeg, MB, Canada. His research focuses on the effects of oil migration and partitioning of oil in sea ice in order to observe the effects of weathering on complex permittivity and normal radar cross section for faster response times concerning oil spill detection.